Quantum teleportation with atoms: quantum process tomography

M. Riebe[1], M. Chwalla[1], J. Benhelm[1], H. Häffner[1,2], W. Hänsel[1], C. F. Roos[1,2] and R. Blatt[1,2]

[1]Institut für Experimentalphysik, Universität Innsbruck, Technikerstrasse 25, A-6020 Innsbruck
[2]Institut für Quantenoptik und Quanteninformation der Österreichischen Akademie der Wissenschaften, Technikerstr. 21a, A-6020 Innsbruck

Abstract. The performance of a quantum teleportation algorithm implemented on an ion trap quantum computer is investigated. First the algorithm is analyzed in terms of the teleportation fidelity of six input states evenly distributed over the Bloch sphere. Furthermore, a quantum process tomography of the teleportation algorithm is carried out which provides almost complete knowledge about the algorithm.

1. Introduction

Quantum teleportation [1] is one of the fundamental experiments of quantum information science. The transfer of the quantum properties of one system to a second (distant) system based on the nonlocal properties of an entangled state highlights the most peculiar and fascinating aspects of quantum mechanics. The experimental realization of teleportation requires complete experimental control over a system's quantum state. For this reason, teleportation has been only implemented in a few physical systems [2–9]. One of these systems are strings of cold ions stored in linear Paul traps. The achievable level of control over the quantum state of trapped ions makes this system an ideal candidate for quantum information processing. Single and two-qubit gates constituting the fundamental building blocks for quantum information processing have already been demonstrated [10–13] and characterized by quantum process tomography [14]. The concatenation of quantum gates in combination with measurements has been used for demonstrating simple quantum algorithms [15–17]. Quantum teleportation can be viewed as an algorithm that maps one ion's quantum state to another ion. In the context of quantum communication, teleportation can also be interpreted as a non-trivial implementation of the trivial quantum channel representing the identity operation. In this paper, we characterize an ion trap based experimental implementation of such a quantum channel by quantum process tomography. We improve the previously reported fidelity of the teleportation operation [8] and extend the analysis by teleporting the six eigenstates of the Pauli operators $\sigma_{x,y,z}$ and measuring

the resulting density matrices. These data are used for reconstructing the completely positive map characterizing the quantum channel.

2. Teleporting an unknown quantum state

Teleportation achieves the faithful transfer of the state of a single quantum bit between two parties, usually named Alice and Bob, by employing a pair of qubits prepared in a Bell state shared between the two parties. The protocol devised by Bennett et al. [1] assumes Alice to be in possession of a quantum state $\psi_{in} = \alpha|0\rangle + \beta|1\rangle$, where α and β are unknown to Alice. In addition, she and Bob share a Bell state given by

$$|\Psi_+\rangle = \frac{1}{\sqrt{2}}\left(|0\rangle_A|1\rangle_B + |1\rangle_A|0\rangle_B\right), \tag{1}$$

where the subscripts indicate whether the qubit is located in Alice's or Bob's subsystem. The joint three qubit quantum state of Alice's and Bob's subsystem

$$|\Psi\rangle_{AB} = \frac{1}{\sqrt{2}}\left(\alpha|00\rangle_A|1\rangle_B + \beta|10\rangle_A|1\rangle_B + \alpha|01\rangle_A|0\rangle_B + \beta|11\rangle_A|0\rangle_B\right) \tag{2}$$

can be rearranged by expressing the qubits on Alice's side in terms of the Bell states $\Psi^\pm = (|10\rangle \pm |01\rangle)/\sqrt{2}$ and $\Phi^\pm = (|00\rangle \pm |11\rangle)/\sqrt{2}$:

$$|\Psi\rangle_{AB} = \frac{1}{2}(\Phi_A^+ \underbrace{(\alpha|1\rangle + \beta|0\rangle)}_{\sigma_x \cdot \Psi_{in}}{}_B + \Phi_A^- \underbrace{(\alpha|1\rangle - \beta|0\rangle)}_{\sigma_z \cdot \sigma_x \cdot \Psi_{in}}{}_B + \Psi_A^+ \underbrace{(\alpha|0\rangle + \beta|1\rangle)}_{\Psi_{in}}{}_B$$

$$+ \Psi_A^- \underbrace{(\beta|1\rangle - \alpha|0\rangle)}_{-\sigma_z \cdot \Psi_{in}}{}_B). \tag{3}$$

By a measurement in the Bell basis, Alice projects Bob's qubit into the states $\sigma_x \cdot \Psi_{in}$, $(\sigma_x \sigma_z) \cdot \Psi_{in}$, Ψ_{in} and $\sigma_z \cdot \Psi_{in}$ depending on the result of the measurement. If Alice passes the measurement result on to Bob, he is able to reconstruct Ψ_{in} by applying the necessary inverse operation of either σ_x, $\sigma_z\sigma_x$, I or σ_z to his qubit.

With trapped ions, it is possible to implement teleportation in a completely deterministic fashion since both the preparation of the entangled state and the complete Bell measurement followed by measurement-dependent unitary transformations are deterministic operations.

3. Experimental setup

In our experimental setup, quantum information is stored in superpositions of the $S_{1/2}(m = -1/2)$ ground state and the metastable $D_{5/2}(m = -1/2)$ state of $^{40}\text{Ca}^+$ ions. The calcium ions are held in a linear Paul trap where they form a linear string with an inter-ion distance of about $5\,\mu\text{m}$. State detection is achieved by illuminating the ion string with light at 397 nm resonant with the $S_{1/2} \leftrightarrow P_{1/2}$-transition and detecting the resonance fluorescence of the ions with a CCD camera or a photo multiplier tube. Detection of the presence or absence of resonance fluorescence corresponds to the cases where an ion has been projected into the $|S\rangle$ or $|D\rangle$-state, respectively. The ion qubits
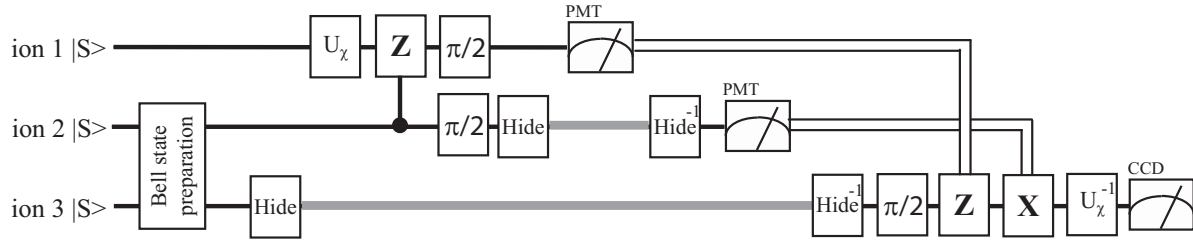
Figure 1. Teleportation algorithm for three ion-qubits. Ion 1 is prepared in the input state $|\chi\rangle = U_\chi |S\rangle$ while ion 2 and 3 are prepared in a Bell state. The teleportation pulse sequence transfers the quantum information to ion 3. During the Bell measurement the quantum information in the ions not subjected to the measurement are protected from the 397 nm light by shifting the $|S\rangle$-state population to an additional $|D\rangle$-substate using the pulses denoted by Hide and Hide^{-1}. The operations labelled X and Z represent spin flip and phase flip operations, respectively.

can be individually manipulated by pulses of a tightly focussed laser beam exciting the $|S\rangle \leftrightarrow |D\rangle$ quadrupole transition at a wavelength of 729 nm. The motion of the ions in the harmonic trap potential are described by normal modes, which appear as sidebands in the excitation spectrum of the $S_{1/2} \leftrightarrow D_{5/2}$ transition. For coherent manipulation, only the quantum state of the axial center of mass mode at a frequency of $\omega_{COM} = 2\pi \times 1.2$ MHz is relevant. Exciting ions on the corresponding upper or blue sideband leads to transitions between the quantum states $|S, n\rangle$ and $|D, n + 1\rangle$, where n is the number of phonons. By employing sideband laser cooling the vibrational mode is initialized in the ground state $|n = 0\rangle$ and can be precisely controlled by subsequent sideband laser pulses. These sideband operations, supplemented by single qubit rotations using the carrier transition, enable us to implement an entangling two-qubit quantum gate. Further details of the experimental setup can be found in [18].

4. Implementing teleportation in an ion trap

Three ion-qubits are sufficient for the teleportation experiment. One qubit carries the unknown quantum information and an entangled pair of qubits provides the necessary entangled resource for the information transfer.

Fig. 1 provides an overview of the pulse sequence used for teleportation. A complete list of all necessary experimental steps is given in Tab. 1. This pulse sequence can be broken down into the following experimental steps:

(i) **Initialization of ion qubits:** Initially, the ion string's vibrational motion is laser-cooled by Doppler cooling on the $S_{1/2} \leftrightarrow P_{1/2}$ dipole transition. Subsequent sideband cooling on the $S_{1/2} \leftrightarrow D_{5/2}$ quadrupole transition initializes the center-of-mass mode in the ground state, which is a crucial prerequisite for the entangling and disentangling sideband operations in the teleportation circuit. By a pulse of circular polarized 397 nm light, we make sure that all ion qubits are in the $S_{1/2}(m = -1/2)$ ground state at the beginning of the teleportation sequence.

(ii) **Bell state preparation:** Ion 2 and 3 are prepared in the Bell state $(|DS\rangle + |SD\rangle)/\sqrt{2}$ by a sequence of three laser pulses (see Tab. 1). We are able to generate this entangled state with a fidelity of up to 96% [19]. Furthermore, this particular Bell state is highly robust with respect to the major decoherence mechanisms in our experimental resulting in a lifetime only limited by the lifetime of the metastable $D_{5/2}$-level [19].

(iii) **Preparation of the input state:** Ion 1 is prepared in the input state $|\psi_{in}\rangle = U_\chi|S\rangle$, where U_χ is a single qubit rotation.

(iv) **Rotation into the Bell-basis:** In order to carry out the measurement in the Bell basis, we have to map the Bell basis onto the product basis $\{|SS\rangle, |SD\rangle, |DS\rangle, |DD\rangle\}$, which is the natural measurement basis in our setup. This basis transformation is achieved by first applying a CNOT gate operation to the qubits, mapping the Bell states onto separable states, and a final Hadamard-like single qubit rotation. In our quantum circuit the CNOT gate, which is extensively described in [18], is decomposed into a controlled phase gate and two single qubit rotations of length $\pi/2$. However, one of the $\pi/2$-rotations (pulse 30 in Tab. 1) is shifted to the reconstruction operations on ion 2. This means that the product basis corresponds to a different set of entangled states, namely $\{(\Phi^- + \Psi^+)/\sqrt{2}, (\Phi^+ + \Psi^-)/\sqrt{2}, (\Phi^+ - \Psi^-)/\sqrt{2}, (\Phi^+ - \Psi^-)/\sqrt{2}\}$ are mapped onto $\{|DD\rangle, |DS\rangle, |SD\rangle, |SS\rangle\}$.

(v) **Selective read-out of the ion string:** Ion 1 and 2 are measured in the product basis by illuminating the ions with light at 397 nm for 250 μs and detecting the presence or absence of resonance fluorescence on the $S_{1/2} \leftrightarrow P_{1/2}$-transition that indicates whether the individual ion was projected into state $|S\rangle$ or $|D\rangle$. During the measurement process the coherence of the target ion 3 has to be preserved. Therefore, the S-state population of ion 3 is transferred to an additional Zeeman sub-state of the $D_{5/2}$ level, which is not affected by the detection light [16]. For the detection of the fluorescence light of ion 1 and 2 we use a photomultiplier (PMT), since its signal can be directly processed by a digital counter electronics which then decides which further reconstruction operations are later applied to ion 3. However, this requires to read out the two ions subsequently as the states $|SD\rangle$ and $|DS\rangle$ cannot be distinguished with the PMT in a simultaneous measurement of both ions. This is implemented measuring one ion while hiding the other ion using the technique described above.

(vi) **Spin-echo rephasing:** Application of the hiding technique to qubit 3 protects the quantum information it carries from the influence of the Bell measurement on the other ions. However, quantum information stored in the D-state manifold is much more susceptible to phase decoherence from magnetic field fluctuations. In order to undo these phase errors a spin echo sequence [20] is applied to qubit 3 (pulse 17 in Tab. 1). In order to let qubit 3 rephase, a waiting time of 300 μs is inserted after completion of the Bell measurement before the reconstruction operations are

applied. Simulations of the teleportation algorithm show that the spin-echo waiting time which maximizes the teleportation fidelity depends on the chosen input state. Since a maximum mean teleportation fidelity is desired, a spin-echo time has to be chosen which is the best compromise between the individual fidelities of the input states. Additionally, we carry out a spin-echo pulse on ion 1 after the phase gate in order to cancel phase shifts during the gate operation.

(vii) **Conditional reconstruction operation:** The information gained in step (v) allows us to apply the proper reconstruction operations for qubit 3. However, compared to the reconstruction operations found in Sec. 2 the preset single qubit rotations in our teleportation circuit have to be modified due to the omitted $\pi/2$-rotation in the Bell measurement and due to the spin echo applied to ion 3 which acts as an additional $-iY$-rotation. First of all an additional $\pi/2$-rotation is applied to ion 3, making up the rotation missing in the Bell analysis. Finally, for the four Bell measurement results $\{|DD\rangle, |DS\rangle, |SD\rangle, |SS\rangle\}$ the single qubit rotations $\{XZ, iX, iZ, I\}$ have to be applied to qubit 3, i.e. a Z-operation has to be applied whenever ion 1 is found in the $|D\rangle$-state and an X-operation whenever ion 2 is found to be in $|D\rangle$. Note that all these single qubit rotations and all following analysis pulses are applied with an additional phase ϕ. This allows us to take into account systematic phase errors of qubit 3, by maximizing the teleportation fidelity for one of the input states by adjusting ϕ [8]. This optimum phase ϕ is then kept fixed when teleporting any other quantum states.

5. Teleportation results

Due to experimental imperfections and interaction of the qubits with the environment, no experimental implementation of teleportation will be perfect. For this reason, we describe the experimental teleportation operation by a completely positive map $\mathcal{E}(\rho)$, expressed in operator sum representation as [21]:

$$\mathcal{E}(\rho) = \sum_{m,n=1}^{4} \chi_{mn} \, A_m \rho A_n^\dagger, \tag{4}$$

where ρ is the input state to be teleported, and $A_m \in \{I, \sigma_x, \sigma_y, \sigma_z\}$ is a set of operators forming a basis in the space of single-qubit operators. The process matrix χ contains all information about the state-mapping from qubit 1 to qubit 3.

A useful quantity characterizing the quantum process $\mathcal{E}$ is the average fidelity $\bar{F} = \int d\psi \langle \psi | \mathcal{E}(\psi) | \psi \rangle$ where the average over all pure input states is performed using a uniform measure on state space with $\int d\psi = 1$. In the case of a single qubit process, the integral would be over the surface of the Bloch sphere. However, for the calculation of $\bar{F}$, an average over a suitably chosen finite set of input states suffices [22, 23]. Using the eigenstates $\psi_{\pm k}, k \in \{x, y, z\}$, of the Pauli matrices $\sigma_x, \sigma_y, \sigma_z$, $\bar{F}$ is obtained by calculating $\bar{F} = \frac{1}{6} \sum_{j \in \{\pm x, \pm y, \pm z\}} \langle \psi_j | \mathcal{E}(\psi_j) | \psi_j \rangle$.

Table 1. Sequence of laser pulses and experimental steps to implement teleportation. Laser pulses applied to the i-th ion on carrier transitions are denoted by $R_i^C(\theta, \varphi)$ and $R_i^H(\theta, \varphi)$ and pulses on the blue sideband transition by $R_i^+(\theta, \varphi)$, where $\theta = \Omega t$ is the pulse area in terms of the Rabi frequency Ω, the pulse length t and its phase φ [19]. The index C denotes carrier transitions between the two logical eigenstates, while the index H labels transitions from the $S_{1/2^-}$ to the additional $D_{5/2}$–Zeeman substate used to hide individual ion qubits.

		Action	Comment
	1	Light at 397 nm	Doppler preparation
	2	Light at 729 nm	Sideband cooling
	3	Light at 397 nm	Optical pumping
Entangle	4	$R_3^+(\pi/2, 3\pi/2)$	Entangle ion #3 with motional qubit
	5	$R_2^C(\pi, 3\pi/2)$	Prepare ion #2 for entanglement
	6	$R_2^+(\pi, \pi/2)$	Entangle ion 2 with ion 3
	7	Wait for 1μs – $10\,000\ \mu$s	Stand–by for teleportation
	8	$R_3^H(\pi, 0)$	Hide target ion
	9	$R_1^C(\vartheta_\chi, \varphi_\chi)$	Prepare source ion #1 in state χ
Rotate into Bell–basis	10	$R_2^+(\pi, 3\pi/2)$	Get motional qubit from ion 2
	11	$R_1^+(\pi/\sqrt{2}, \pi/2)$	Composite pulse for phasegate
	12	$R_1^+(\pi, 0)$	Composite pulse for phasegate
	13	$R_1^+(\pi/\sqrt{2}, \pi/2)$	Composite pulse for phasegate
	14	$R_1^+(\pi, 0)$	Composite pulse for phasegate
	15	$R_1^C(\pi, \pi/2)$	Spin echo on ion 1
	16	$R_3^H(\pi, \pi)$	Unhide ion 3 for spin echo
	17	$R_3^C(\pi, \pi/2)$	Spin echo on ion 3
	18	$R_3^H(\pi, 0)$	Hide ion 3 again
	19	$R_2^+(\pi, \pi/2)$	Write motional qubit back to ion #2
	20	$R_1^C(\pi/2, 3\pi/2)$	Part of rotation into Bell–basis
	21	$R_2^C(\pi/2, \pi/2)$	Finalize rotation into Bell basis
Read–out	22	$R_2^H(\pi, 0)$	Hide ion 2
	23	PMT detection #1 (250 μs)	Read out ion 1 with photomultiplier
	24	$R_1^H(\pi, 0)$	Hide ion 1
	25	$R_2^H(\pi, \pi)$	Unhide ion 2
	26	PMT detection #2 (250 μ)s	Read out ion 2 with photomultiplier
	27	$R_2^H(\pi, 0)$	Hide ion #2
	28	Wait 300 μs	Let system rephase; part of spin echo
	29	$R_3^H(\pi, \pi)$	Unhide ion 3
	30	$R_3^C(\pi/2, 3\pi/2 + \phi)$	Change basis
Recon-struction	31	$R_3^C(\pi, \phi)$	$\left.\begin{array}{l}\mathrm{i}\sigma_x\\ \text{-}\mathrm{i}\sigma_y\end{array}\right\} = -i\sigma_z$ conditioned on PMT detection #1
	32	$R_3^C(\pi, \pi/2 + \phi)$	
	33	$R_3^C(\pi, \phi)$	$\mathrm{i}\sigma_x$ conditioned on PMDetection 2
	34	$R_3^C(\vartheta_\chi, \varphi_\chi + \pi + \phi)$	Inverse of preparation of χ with offset ϕ
	35	Light at 397 nm	Read out ion 3 with camera

The overlap $\langle\psi_j|\mathcal{E}(\psi_j)|\psi_j\rangle$ between the input state ψ_j prepared in ion qubit #1 with the output state generated via teleportation in ion qubit #3 is measured directly in our experiment by applying the inverse unitary transformation to ion qubit #3 after teleportation and determining the probability to find this qubit in the initial state $|S\rangle$, i.e. formally the teleportation fidelity is given by $F_{tele} = \langle S|U_\chi^{-1}\rho_{exp}U_\chi|S\rangle$, where ρ_{exp} is the quantum state of ion qubit #3 after teleportation. For the six input states $\psi_1 = |S\rangle$, $\psi_2 = |D\rangle$, $\psi_3 = (|D\rangle - i|S\rangle)/\sqrt{2}$, $\psi_4 = (|D\rangle - |S\rangle)/\sqrt{2}$, $\psi_5 = (|D\rangle + i|S\rangle)/\sqrt{2}$, $\psi_6 = (|D\rangle + |S\rangle)/\sqrt{2}$, the teleportation fidelities range between 79% and 87% (see Fig. 2), with an average fidelity of $\bar{F} = 83(1)\%$. This average fidelity proves successful operation of the teleportation algorithm, as it exceeds the maximum value of 2/3 that is achievable without using entangled states [24].
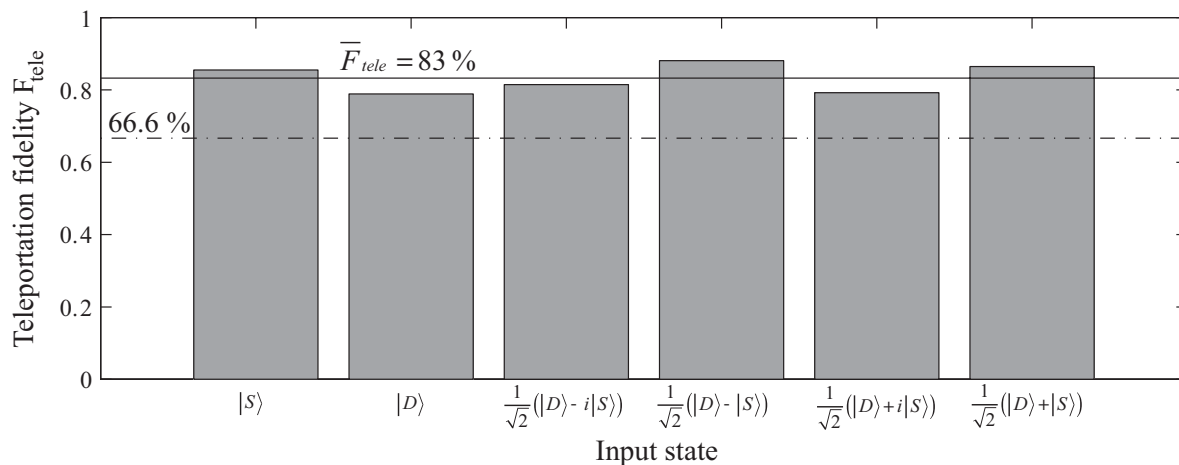

Figure 2. Measured teleportation fidelity F_{tele} for six different input states. All fidelities are well above the 2/3 threshold proving successful quantum teleportation. The average teleportation fidelity is $\bar{F}_{tele} = 83(1)\%$.

A more complete way of characterizing the teleportation process is achieved by determining the output state of qubit 3 by quantum state tomography, which requires measurements in three different measurement bases. From these measurements, the density matrix of the output qubit is estimated using a maximum likelihood algorithm [19]. The resulting density matrices of the six input states are shown in Fig. 3.

Full information about the relation between the input and output of the teleportation algorithm is gained by a quantum process tomography. This procedure requires to determine the output state $\mathcal{E}(\rho_i)$ after application of the investigated operation for a set of at least four linear independent input states ρ_i. With this data, the process matrix χ is obtained by inverting equation (4). Due to inevitable statistical errors in the measurement process the resulting χ will in general not be completely positive. This problem is avoided by employing a maximum likelihood algorithm, which determines the completely positive map which yields the highest probability of producing the measured data set. We use the tomographically reconstructed input states ψ_1-ψ_6 for a determination of the process matrix χ by maximum likelihood estimation [25].
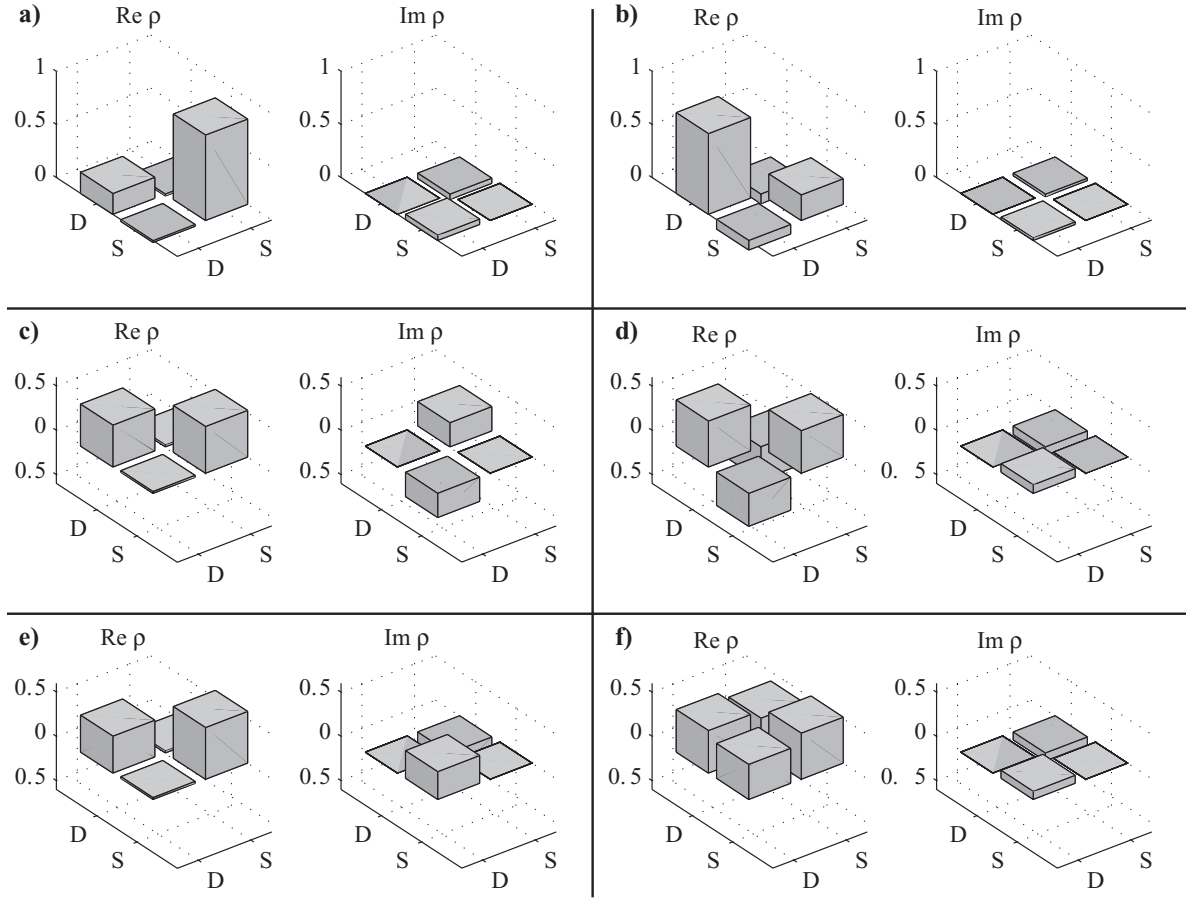
Figure 3. Real and imaginary part of the density matrix of the output qubit for the six different input states a) $\psi_1 = |S\rangle$, b) $\psi_2 = |D\rangle$, c) $\psi_3 = (|D\rangle - i|S\rangle)/\sqrt{2}$, d) $\psi_4 = (|D\rangle - |S\rangle)/\sqrt{2}$, e) $\psi_5 = (|D\rangle + i|S\rangle)/\sqrt{2}$, f) $\psi_6 = (|D\rangle + |S\rangle)/\sqrt{2}$.

The absolute value of the elements of the resulting process matrix χ_{tele} is shown in Fig. 4a). As expected, the dominant element is the identity with $\chi_{II} = 0.73(1)$, which is identical to the process fidelity $F_{proc} = tr(\chi_{idtele}\chi_{tele})$, where χ_{idtele} denotes the ideal process matrix of the teleportation algorithm. This agrees well with the average fidelity stated above, as average and process fidelity are related by $\bar{F} = (2F_{proc} + 1)/3$ for a single qubit map [23].

A quantum process operating on a single quantum bit can be conveniently represented geometrically by picturing the deformation of a Bloch sphere subjected to the quantum process [21]. The quantum operation maps the Bloch sphere into itself by deforming it into an ellipsoid that may be rotated and displaced with respect to the original sphere representing the input states. This transformation is described by an affine map $r_{out} = OSr_{in} + b$ between input and output Bloch vectors where the matrices O and S are orthogonal and positive-semidefinite, respectively. Fig. 4b) shows the result for the teleportation algorithm. The transformed ellipsoid is centered at $b \approx (0, 0.09, -0.05)$ with errors of about ± 0.03 for each coordinate. The matrix S shrinks the sphere anisotropically (its eigenvalues are 0.78, 0.58, 0.55), O rotates the
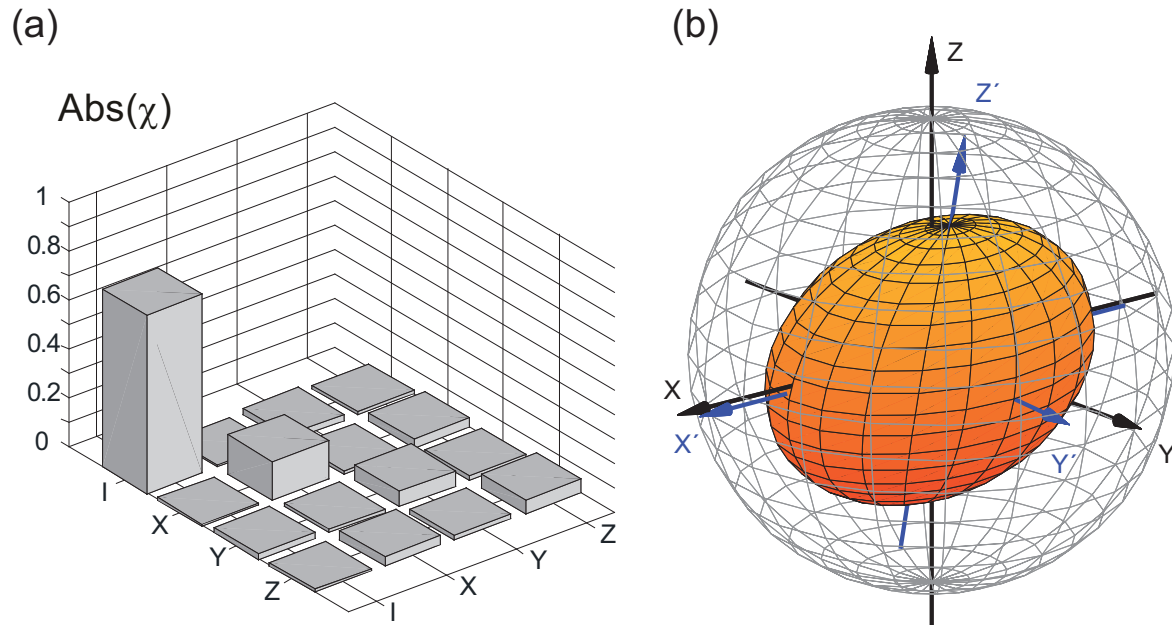
(a)

(b)

Figure 4. Results of process tomography of teleportation algorithm. In (a) the absolute value of process matrix χ is shown. The dominating diagonal element is the identity with $\chi_{II} = 0.73(1)$. The plot drawn in (b) shows how the input states lying on the surface of the initial Bloch sphere (meshed surface) are transformed by the teleportation algorithm, with the output states lying on the solid surface.

sphere by an angle of about $2°(2)$. This demonstrates that the loss of fidelity is mostly due to decoherence and not caused by an undesired unitary operation rotating the sphere as the orientation of the deformed Bloch sphere hardly differs from the orientation of the initial sphere. The results are consistent with the assumption that the rotation matrix O is equal to the identity as desired.

6. Conclusion

We demonstrated deterministic teleportation of quantum information between two atomic qubits. We improve the mean teleportation fidelity $\bar{F} = 75\%$ reported in [8] to $\bar{F} = 83(1)\%$ and unambiguously demonstrate the quantum nature of the teleportation operation by teleporting an unbiased set of six basis states [26] and using the data for completely characterizing the teleportation operation by quantum process tomography. The process tomography result shows that the main source of infidelity is decoherence while systematic errors are negligible. To make further progress towards high-fidelity quantum operations, decoherence rates have to be reduced by either reducing environmental noise or encoding quantum information in noise-tolerant quantum states [27].

References

[1] Bennett C H, Brassard G, Crépeau C, Jozsa R, Peres A, and Wootters W K 1993, Phys. Rev. Lett. **70**, 1895

[2] Bouwmeester D, Pan J–W, Mattle K, Eible M, Weinfurter H, and Zeilinger A 1997 Nature **390** 575

[3] Boschi D *et al.* 1998 Phys. Rev. Lett. **80** 1121

[4] Furusawa A *et al.* 1998 Science **282** 706

[5] Nielsen M A, Knill E, and Laflamme R 1998 Nature **396** 52

[6] Pan J.-W. *et al.* 2001 Phys. Rev. Lett. **86** 4435

[7] Marcikic I, de Riedmatten H, Tittel W, Zbinden H, and Gisin N 2003 Nature **421** 509

[8] Riebe M *et al.* 2004 Nature **429** 734

[9] Barrett M D *et al.* 2004, Nature **429** 737

[10] Leibfried D *et al.* 2003 Nature **422** 412

[11] Schmidt–Kaler F *et al.* 2003 Nature **422** 408

[12] Haljan P C *et al.* 2005 Phys. Rev. A **72** 062316

[13] Home J P *et al.* 2006 New J. Phys. **8** 188

[14] Riebe M *et al.* 2006 Phys. Rev. Lett. **97** 220407

[15] Gulde S *et al.* 2003 Nature **421** 48

[16] Roos C F *et al.* 2004 Science **304** 1478

[17] Reichle R *et al.* 2006 Nature **443** 838

[18] Schmidt-Kaler F *et al.* 2003 Appl. Phys. B **77** 789

[19] Roos C F *et al.* 2004 Phys. Rev. Lett. **92** 220402

[20] Hahn E L 1950 Phys. Rev. **77** 746

[21] Nielsen M A, and Chuang I L 2000 *Quantum Computation and Quantum Information*, Cambridge University Press, Cambridge

[22] Bowdrey M D, Oi D K L, Short A J, Banaszek K, and Jones J A 2002 Phys. Lett. A **294** 258

[23] Nielsen M A 2002 Phys. Lett. A **303** 249

[24] Massar S, Popescu S 1995 Phys. Rev. Lett. 74, 12591263

[25] Ježek M, Fiurášek J and Hradil Z 2003, Phys. Rev. A **68** 012305

[26] van Enk S J, Lütgenhaus N, and Kimble H J, *Preprint* quant-ph/0611219

[27] Langer C *et al.* 2005 Phys. Rev. Lett **95** 060502